King Saud University

Arabian Journal of Chemistry

www.ksu.edu.sa
www.sciencedirect.com

ORIGINAL ARTICLE

Co-immobilization of clinoptilolite and nanostructured hydrated ferric-zirconium binary oxide via polyvinyl alcohol-alginate covalent cross-linking for simultaneous deep removal of aqueous low-level nitrogen and phosphorus

Kun Zhou [a,b], Boran Wu [a,c,*], Xiaoli Chai [a,c], Xiaohu Dai [a,c]

[a] State Key Laboratory of Pollution Control and Resource Reuse, College of Environmental Science and Engineering, Tongji University, 1239 Siping Road, Shanghai 200092, China
[b] Shanghai Municipal Engineering Design Institute (Group) Co. Ltd., 901 North Zhongshan Road, Shanghai 200092, China
[c] Shanghai Institute of Pollution Control and Ecological Security, 1239 Siping Road, Shanghai 200092, China

Abstract A novel absorbent, PVA/SA-CFZ, was developed by jointly enveloping nanostructured hydrated ferric-zirconium binary oxide and clinoptilolite in the cross-linking of polyvinyl alcohol (PVA)/sodium alginate (SA). As a result, the cation exchange capacity of clinoptilolite and electrostatic attraction capacity of hydrated ferric-zirconium binary oxide can be integrated for the simultaneous removal of nitrogen and phosphorus from wastewater. The adsorption behavior of PVA/SA-CFZ for the co-existing ammonium and phosphate was primarily investigated by batch experiments. Over a wide pH range (4 ~ 11), PVA/SA-CFZ always showed the excellent adsorption performance both for the low-concentration ammonium (< 5 mg/L) and phosphate (< 0.5 mg/L), which reflected the well adaptability towards unfavorable environmental conditions. The kinetic analysis indicated that the pseudo-second-order kinetic model could quantitatively describe the adsorption process optimally. The mechanistic investigation revealed that ammonium was captured through the cation exchange reaction with clinoptilolite. The electrostatic attraction, inner sphere complexation with Fe/Zr-O-OH groups, and formation of phosphate precipitation jointly

* Corresponding author at: State Key Laboratory of Pollution Control and Resource Reuse, College of Environmental Science and Engineering, Tongji University, 1239 Siping Road, Shanghai 200092, China.
  E-mail address: boranwu@tongji.edu.cn (B. Wu).
Peer review under responsibility of King Saud University.

Production and hosting by Elsevier

contributed to the fixation of phosphate by PVA/SA-CFZ. Generally, it is believed that PVA/SA-CFZ can serve as a promising composite absorbent for the simultaneous deep removal of nitrogen and phosphorus, and support for the advanced treatment of wastewater containing low-level nutrients.

1. Introduction

Nitrogen and phosphorus are two essential nutrients for plant and microbial growth, however, the excess nitrogen and phosphorus could cause adverse impact on the water quality and the balance of aquatic ecosystem, thus resulting in eutrophication (Liu et al., 2018). Hence, the effective reduction of nitrogen and phosphorus is of considerably significance to counteract the occurrence of eutrophication, especially in some environmentally sensitive regions requiring ultra-low pollution loads. Currently, several valuable technologies for removing nitrogen and phosphorus have been proposed, including biological nutrient removal (Adrian et al., 2007), chemical precipitation (Lin et al., 2015), and adsorption (Ko et al., 2016). It is reported that the efficiency of conventional biological nutrient removal could be highly vulnerable to operational conditions, and chemical precipitation consumes a large amount of unrecyclable chemicals and is unable to remove phosphorus below 100 μg/L (Bacelo et al., 2020; Blaney et al., 2007). On the contrary, the adsorption has been proven to be the ideal supplement to biological nutrient removal and chemical precipitation due to its potentials in fairly simple operation, relatively low dosage, abundant absorbent materials and effective adaptivity to varied environmental conditions (Bui et al., 2018; Tu et al., 2019).

Developing eco-friendly, highly-efficient, and economical absorbents is primarily essential for both adsorption-based nutrient recovery and advanced treatment of wastewater towards ultra-low discharge standards. Recently, numerous materials have been explored as the nitrogen and phosphorus absorbents including zeolites (Wan et al., 2017), activated carbon (Qi et al., 2012), blast furnace slag (Gong et al., 2009; Oguz, 2004), metal oxides (Hu et al., 2018), and so on. However, the application of activated carbon and blast furnace slag is limited by their operation cost and potential environmental risks (i.e. the application of blast furnace slag could lead to the increase in pH value). Particularly, zeolites have been considered as promising materials for water treatment owing to non-toxicity, high removal efficiency, and economical advantages. As one of the most abundant natural zeolites, clinoptilolite comprises the microporous structure of a three-dimensional framework of alumina and silica (Li et al., 2019). Distinctive spatial structure endows clinoptilolite with some valuable physical–chemical properties such as cation exchange, catalysis, and molecular sieving (Wan et al., 2017). Results of several previous studies have also proposed clinoptilolite as excellent absorbent material for ammonium and heavy metal removal through cation exchange mechanism (Cui et al., 2006; Vassileva and Voikova, 2009). However, the negatively-charged framework of clinoptilolite restrains the affinity for anionic species, for example, phosphate.

On the other hand, it has been verified that metal (hydro) oxides (namely hydrous iron oxides, hydrous lanthanum oxides, and hydrous manganese oxide) can be modified to develop the effective and promising absorbent for remediating phosphate pollution (Lai et al., 2016; Rashidi Nodeh et al., 2017). Metal (hydro) oxides exhibit preferential ligand sorption towards phosphate through forming inner-sphere complexes based on Lewis acid-base interactions (Acelas et al., 2015). In comparison with other metal (hydro) oxides, hydrous iron oxides and hydrous zirconium oxides have been proven to have the higher sorption affinity for phosphate with the advantage of innocuity and strong chemical stability (Bui et al., 2018; Zhang et al., 2019a). Nevertheless, the application of these metal (hydro) oxides in native form was restricted owing to lack of mechanical strength and attrition resistance properties (Blaney et al., 2007), and therefore appropriately loading metal (hydro) oxides on the supporting structure is quietly demanded.

The chemical cross-linking with polyvinyl alcohol (PVA)/sodium alginate (SA) and boric acid can be used as an effective assembling approach for composites. As an immobilization matrix, PVA is a synthetic water-soluble hydrophilic polymer with desirable characteristics including chemical stability, non-toxicity, and lower cost (Abd El-aziz et al., 2016; Shilin et al., 2018). During the cross-linking process, boric acid acts as cross-linker and boron bonds connected with four molecules of PVA to form a monodiol type PVA-boric acid viscoelastic gel, and the addition of SA would increase the surface area and mechanical strength of synthesized gel products (Bae et al., 2017). Nowadays, little research has been conducted on the application of PVA/SA and boric acid to co-immobilize natural zeolite materials and metal oxides. The potential of composite integrating zeolite and metal oxides for simultaneous nitrogen and phosphorus removal is worth to be explored.

Based on the cross-linking process of PVA/SA and boric acid, this study aimed to realize the co-immobilization of clinoptilolite and hydrous iron-zirconium oxides, and accordingly fabricate a novel absorbent named PVA/SA-CFZ. The physiochemical properties of PVA/SA-CFZ including microtopography, crystal constituents and pore structure were primarily characterized. Furthermore, the performance of PVA/SA-CFZ for simultaneous removal of aqueous nitrogen and phosphorus was evaluated, and the in-depth investigation on relevant mechanisms were also conducted. The superior performance of PVA/SA-CFZ towards low-concentration nitrogen and phosphorus was found in this study, which should support its great potentials in advanced treatment of

effluent of wastewater treatment plants for environmentally sensitive areas.

2. Materials and methods

2.1. Chemicals

Clinoptilolite was available from Gongyi Mines Co., Henan, China. After washed three times with deionized water and dried in oven at 80 ℃ for 24 h, clinoptilolite was ground into powders. All the chemicals used in this study were analytical grade unless otherwise stated. Iron (II) sulfate heptahydrate ($FeSO_4 \blacksquare 7H_2O$), ammonium chloride ($NH_4Cl$), sodium hydroxide (NaOH, slice), and calcium chloride anhydrous ($CaCl_2$) were purchased from Shanghai Maclin Biochemical Technology Co., Ltd, Shanghai, China. Zirconyl chloride octahydrate ($ZrOCl_2 \blacksquare 8H_2O$), sodium phosphate monobasic dehydrate ($NaH_2PO_4 \blacksquare 2H_2O$), polyvinyl alcohol (PVA), sodium alginate ($(C_6H_7O_6Na)_n$, SA), and boric acid (H_3BO_3) were provided by Aladdin Biochemical Technology Co., Ltd, Shanghai, China. Exactly, 0.5032 g $NaH_2PO_4 \blacksquare 2H_2O$ and 0.3820 g NH_4Cl were added into 1 L ultrapure water for preparing 100 mg P/L phosphorus stock solution and 100 mg N/L nitrogen stock solution, respectively. A mixture solution of H_3BO_3 (5 wt%) and $CaCl_2$ (2 wt%) was prepared by dissolving 50 g H_3BO_3 and 20 g $CaCl_2$ into 1 L ultrapure water.

2.2. Preparation of PVA/SA-CFZ

The preparation of PVA/SA-CFZ was performed by cross-linking process, which can be briefly stated as following: First, PVA (10 g) and SA (2 g) were completely dissolving in 100 mL hot water (100 ℃) with constantly stirring. Second, with continuous agitation and 60 ℃ hot-water bath, hydrated ferric-zirconium binary oxide precipitate was generated by slowly adding 1 mol/L NaOH into the mixture solution of $FeSO_4 \blacksquare 7$-H_2O (0.5 mol/L) and $ZrOCl_2 \blacksquare 8H_2O$ (0.5 mol/L) to allow the complete hydroxylation. Third, the obtained hydrated ferric-zirconium binary oxide precipitate and clinoptilolite powder (20 g) were added into the above solution of PVA and SA. After stirred uniformly, the resulted solution was dropped into a mixed solution of H_3BO_3 (5 wt%) and $CaCl_2$ (2 wt%) and then the cross-linking process was induced, during which a novel spherical absorbent named PVA/SA-CFZ could be obtained.

2.3. Characterization of PVA/SA-CFZ

2.3.1. Transmission electron microscopy

Transmission electron microscopy (TEM, Tecnai G2 F20 S-Twin, FEI Co., USA) was applied to analyze the micro-morphology of raw clinoptilolite and PVA/SA-CFZ, which were recorded at 200 kV and resolution of 0.24 nm. The energy-dispersive spectroscopy (EDS, X-Max 80 T detector, Oxford Instruments Ltd., UK) was used to analyze the elemental composition of raw clinoptilolite and PVA/SA-CFZ. The image processing software, Nano measurer 1.2, was used to determine the particle size distribution of nanoparticles identified in TEM images.

2.3.2. Porosity analysis

The porosities of raw clinoptilolite, synthesized PVA/SA-CFZ, and used PVA/SA-CFZ were evaluated by N_2 adsorption at 77 K using a Micromeritics model ASAP-2020 analyzer. The samples were first degassed for 4 h at 573 K to remove any moisture or adsorbed contaminants that might be present on their surface. The surface area was calculated by Brunauer-Emmett-Teller (BET) model. The total pore volume and pore size were estimated using the manufacturer's software by the Barrett-Joyner-Halenda (BJH) method (Barrett et al., 1951).

2.3.3. X-ray diffraction

In order to identify the crystal compositions of PVA/SA-CFZ, D8 ADVANCE powder diffractometer (Bruker AXS Inc., Germany) employing Cu Kα radiation (40 kV, 40 mA) was used to record the X-ray diffraction (XRD) patterns at wavelength of 0.154 nm. The 2θ range was 10 ~ 90° and the scanning speed was 0.1°/min. MDI Jade 6.0 software was used to analyze the resulting diffractograms.

2.3.4. Fourier transform infrared spectroscopy

The functional groups of PVA/SA-CFZ were identified by Fourier transform infrared spectroscopy (FT-IR, Nicolet 5700 FTIR Spectrometer) with the wavenumber range of 500 ~ 4000 cm^{-1} at a resolution of 4 cm^{-1}.

2.3.5. X-ray photoelectron spectroscopy

Thermo Scientific K-Alpha[+] XPS system (Thermo Fisher Scientific Inc., USA) equipped with an Al Kα X-ray monochromator was used to obtain X-ray photoelectron spectroscopy (XPS) spectra of raw clinoptilolite, PVA/SA-CFZ, and PVA/SA-CFZ post phosphate adsorption. The background pressure was maintained at 10^{-6} Pa during data acquisition. The high-resolution Fe2p, Zr3d and O1s region were recorded at a pass energy of 200 eV. The spectra were fitted by XPS peak 4.0 software.

2.4. Adsorption experiments

The adsorption behavior of nitrogen and phosphorous on PVA/SA-CFZ was investigated through batch experiments. In order to examine the adaptability of PVA/SA-CFZ for the advanced treatment of effluent of wastewater treatment plants, the common discharge limits, 0.5 mg phosphate/L and 5 mg ammonium/L, were selected as the initial concentrations for batch experiments in this study (Chinese Ministry of Environmental Protection, 2002; Loos et al., 2012; USEPA, 2008; Weirich et al., 2011). Regarding to the effect of pH values, the investigated initial pH of target solutions containing phosphate and ammonium was first adjusted to the pre-determined values (3, 4, 5, 6, 7, 8, 9, 10 and 11) by using 1 mol/L NaOH and 1 mol/L HCl; then, 0.7 g PVA/SA-CFZ was added into 100 mL of the above solution and the reaction time was set as 12 h. For the effect of absorbent dosage on nitrogen and phosphorus removal efficiencies, 0.2, 0.3, 0.4, 0.5, 0.6, 0.7, 0.8, 0.9 and 1.0 g PVA/SA-CFZ were used for 100 mL solution containing 0.5 mg phosphate/L and 5 mg ammonium/L at the initial pH of 7 ± 0.5, respectively. The kinetic experiments were also conducted at the initial pH of 7 ± 0.5; 6 g PVA/SA-CFZ was added into the 1 L solution

containing 100 mg phosphate/L and 100 mg ammonium/L; the samples were collected at the pre-determined time interval. All the collected samples were immediately filtered through 0.45 μm Teflon filter cartridges and the concentrations of residual phosphate and ammonium were measured using Hach colorimetric assays (Hach Company, Loveland, CO) (Hach, 2002). The chemical species of aqueous nitrogen and phosphorus, including $NH_3 \blacksquare H_2O$, NH_4^+, H_3PO_4, $H_2PO_4^-$, HPO_4^{2-} and PO_4^{3-} under different pH values were simulated by Visual MINTEQ software (US EPA). All the above experiments were conducted in triplicate.

3. Results and discussion

3.1. Characterization of PVA/SA-CFZ

3.1.1. Microtopography

The microtopography and elemental composition of raw clinoptilolite and PVA/SA-CFZ were investigated using TEM and EDS, as shown in Fig. 1. The prismatic lamellar crystal was the dominant feature of raw clinoptilolite. The typical layer-to-layer distance of raw clinoptilolite was observed to be in the range of 0.8 ~ 1.7 nm (Fig. 1a). In term of PVA/SA-CFZ, the cross-linking reaction between PVA and SA resulted in the smooth coating layer for clinoptilolite, but some nanoscale particles could be visually identified under coating layer and filled in the gaps among clinoptilolite crystals. Based on the scale of Fig. 1, the particle size distribution of nanoparticles was determined to range from 70 to 240 nm, and the average particle size was measured to be 120 nm. According to the EDS results, the fractions of Fe and Zr at surface of PVA/SA-CFZ could be as high as 8.32 wt% and 33.23 wt%, respectively. The occurrence of Fe and Zr as the surface ele-

ments of these nanoscale particles in PVA/SA-CFZ reflected the successful formation of hydrated ferric-zirconium binary oxide, which was similar to our previous studies (Zhou et al., 2018). The TEM images of PVA/SA-CFZ also verified that the PVA/SA enveloping effect could realize the dispersion of hydrated ferric-zirconium binary oxide on the surface of clinoptilolite, which provided the adsorption sites for phosphate.

3.1.2. Crystal constituent and surface functional group

The XRD pattern of the PVA/SA-CFZ with a 2θ range between 5° and 90° is depicted in Fig. 2a. The most significant peaks at 2θ = 9.872°, 11.171°, 13.090°, 26.318°, 28.203°, 30.035° and 32.753° were attributed to clinoptilolite, confirming that the major constituents of PVA/SA-CFZ were the typical Na, K and Ca clinoptilolite phases. Furthermore, the peaks with 2θ values of 26.988° and 36.236° could be observed, which directed to the reflection of FeOOH. The peaks at 2θ of 29.228° and 49.583° are assigned to ZrOOH, which verified the successful synthesis of zirconium hydroxyl oxide.

The surface hydroxyl functional groups of PVA/SA-CFZ were examined by FT-IR analysis. According to the spectrum shown in Fig. 2b, the broad peak at 3400 cm^{-1} should correspond to the stretching vibrations of hydroxyl group (–OH) (Naushad, 2014). The strong peak at 1058.5 cm^{-1} could be attributed to the bending vibration of the hydroxyl groups (–OH) of iron/zirconium (hydro) oxides (Wang et al., 2020; Zhang et al., 2007), which was consistent with the previous literatures related to hydroxyl oxides (Prabhu et al., 2017). Hence, these results confirm that hydrated ferric-zirconium binary oxide were successfully formed in the synthesized PVA/SA-CFZ. The protonated surface hydroxyl group grafted to ferric-zirconium atoms could be the complexing sites for
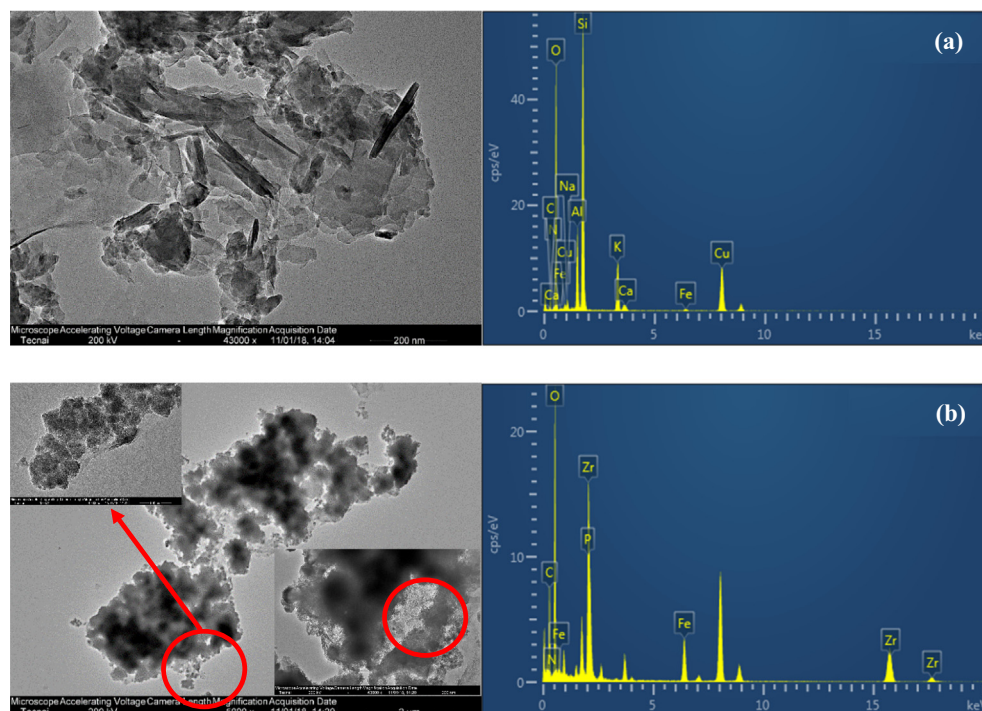
Fig. 1 TEM images and EDS spectra of (a) raw clinoptilolite and (b) synthesized PVA/SA-CFZ.
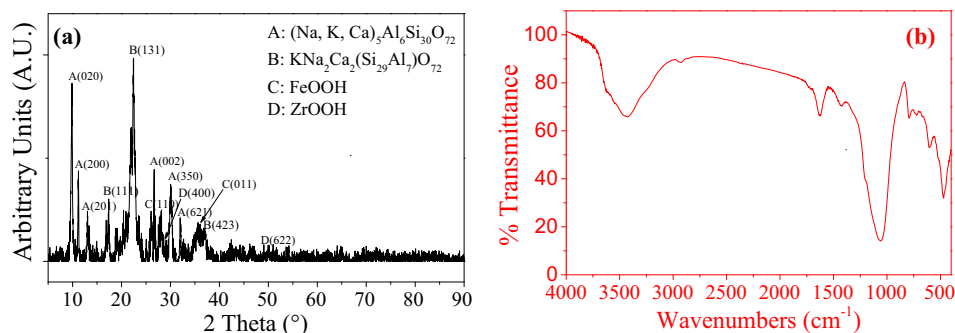
Fig. 2 XRD pattern (a) and FT-IR spectrum (b) of synthesized PVA/SA-CFZ.

phosphorus fixation by electrophilic adsorption (Zhang et al., 2019b).

3.1.3. Pore structure

Table 1 summarizes the microstructure information of raw clinoptilolite and PVA/SA-CFZ. As compared with raw clinoptilolite, the BET surface area of PVA/SA-CFZ before adsorption (i.e. 48.722 m^2/g) was higher than that of raw clinoptilolite (i.e. 33.286 m^2/g). The significant increase proved that the cross-linking process of PVA and boric acid was able to improve the surface feature of raw clinoptilolite and strengthen the adsorption properties of the absorbent PVA/SA-CFZ. Coupled with the rise of BET surface area, the pore size of PVA/SA-CFZ slightly decreased after cross-linking process as compared with raw clinoptilolite. This could be the result of the immobilization of hydrous iron-zirconium oxides in raw clinoptilolite.

3.2. Performance of PVA/SA-CFZ for aqueous nitrogen and phosphorus removal

3.2.1. Effect of initial pH on nitrogen and phosphorus removal

The chemical species of aqueous nitrogen and phosphorus, including $NH_3 \blacksquare H_2O$, NH_4^+, H_3PO_4, $H_2PO_4^-$, HPO_4^{2-} and PO_4^{3-}, significantly rely on pH. Consequently, it is quite demanded to investigate the effect of pH on the simultaneous removal of nitrogen and phosphorus by PVA/SA-FZC. **Figure S1** of **Supplementary Material**s depicts the distribution of nitrogen and phosphorus species under different pH conditions. As shown in **Figure S1a**, the pKa value of ammonium is 9.25. Under the acidic condition, ammonium nitrogen mainly occurs in the ionic form (NH_4^+) (approximately 100%); with the solution pH above pKa, ammonium nitrogen exists in the molecular form ($NH_3 \blacksquare H_2O$) more than the ionic form (NH_4^+). Accordingly, the removal efficiencies of nitrogen under acidic conditions were significantly higher than those under alkaline conditions (Fig. 3a). The removal efficiency of ammonium reached the maximum value at pH of 7, and when pH further rose, the removal efficiency of nitrogen gradually

decreased. This could be attributed to the conversion from NH_4^+ into $NH_3 \blacksquare H_2O \cdot NH_3 \blacksquare H_2O$ was hardly fixed by the modified clinoptilolite based on the mechanism of cation exchange. On the contrary, the phosphorus removal efficiency increased constantly with the increasing pH value. Under alkaline conditions, the dissociation of phosphate makes it negatively charged, which should be in favor of the electrophilic adsorption by the protonated hydroxyl group of ferric-zirconium (hydro) oxides (Zhou et al., 2018).

3.2.2. Effect of absorbent dosage on nitrogen and phosphorus removal

The removal efficiencies of nitrogen and phosphate with different PVA/SA-CFZ dosages are illustrated in Fig. 4a. The removal efficiencies of nitrogen rose from 42.1 ± 3.5% to 99.0 ± 4.3% as the dose of PVA/SA-CFZ increased from 2 g/L to 8 g/L, which was due to the increase in ion-exchange sites for NH_4^+. Also, the adsorption rate should increase with the rising dosage of PVA/SA-CFZ. Therefore, within a specific reaction time (12 h), the substantial increase of nitrogen removal efficiency was observed with PVA/SA-CFZ dosage increasing from 7 g/L to 8 g/L. Similarly, the increase of phosphate removal efficiency was also observed with the dosage of PVA/SA-CFZ increasing from 2 g/L to 6 g/L. However, no significant change in phosphorus removal efficiency was found with PVA/SA-CFZ dosages higher than 5 g/L. Accordingly, the adsorption capacity of PVA/SA-CFZ for phosphate could be calculated as 0.125 ~ mg phosphate/g PVA/SA-CFZ towards the low-concentration phosphorus (~0.5 mg/L), which was higher than those of adsorption experiments conducted under similar conditions (Chen et al., 2015; Xi et al., 2021). That phenomenon confirmed the superior performance of PVA/SA-CFZ for advanced treatment of wastewater.

3.2.3. Kinetic test

Theoretically, the adsorption process is comprised of four steps: external diffusion, intra-particle diffusion, adsorption, and equilibrium (Zong et al., 2017). Kinetic experiments were

Table 1 Porosity of raw clinoptilolite and PVA/SA-CFZ.

	BET surface area (m^2/g)	Pore volume (cm^3/g)	Pore size (nm)
Raw clinoptilolite	33.286 ± 1.295	0.110 ± 0.009	8.211 ± 0.541
PVA/SA-CFZ	48.722 ± 2.510	0.098 ± 0.003	5.044 ± 0.197
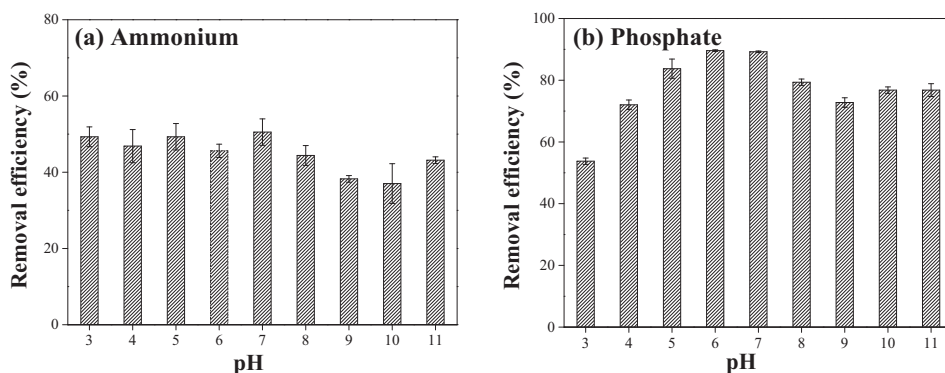
Fig. 3 Effect of pH on the simultaneous removal of (a) ammonium and (b) phosphate by PVA/SA-CFZ. Experimental conditions: initially, 5 mg/L ammonium and 0.5 mg/L phosphate in water; the dosage of PVA/SA-CFZ was 7 g/L; the reaction time was 12 h. Error bars represent min/max values observed for duplicate experiments (too small if not shown).
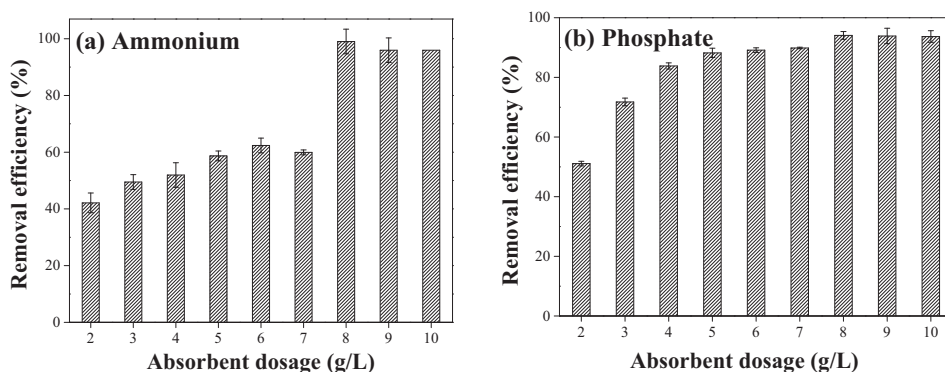
Fig. 4 Effect of absorbent dosage on the simultaneous removal of (a) ammonium and (b) phosphate by PVA/SA-CFZ. Experimental conditions: initially, 5 mg/L ammonium and 0.5 mg/L phosphate in water; the reaction time was 12 h. Error bars represent min/max values observed for duplicate experiments (too small if not shown).

conducted to identify the rate-controlling step of the nitrogen and phosphorus adsorption. Since the nitrogen and phosphorus should be excessive relative to the absorbent (PVA/SA-CFZ) in the kinetic experiments, the results were fitted with two widely used models including pseudo-first-order model and pseudo-second-order model (Fig. 5) (Hill and Root, 2014; Table 2 displayed the corresponding fitting parameters. Based on the correlation coefficients (R^2), the pseudo-second-order model (R^2 = 0.9809–0.9923) simulated the nitro-

gen and phosphorus adsorption better than the pseudo-first-order model (R^2 = 0.9428–0.9920), which reflected that the nitrogen and phosphorus adsorption on PVA/SA-CFZ was primarily controlled by the chemical adsorption instead of the physical adsorption (Wang and Guo, 2020). In addition, the observation of Fig. 5 showed that the nitrogen adsorption process took less time to reach the adsorption equilibrium than the phosphorus adsorption process, which could be attributed to that the rate of cation exchange for ammonium fixation was
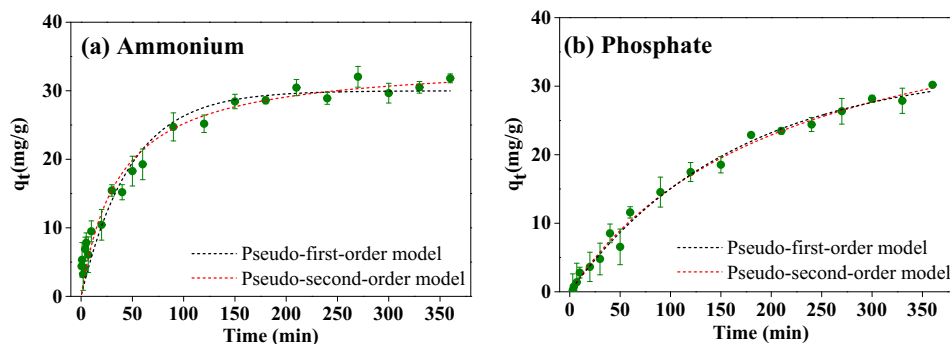
Fig. 5 Adsorption kinetics of (a) ammonium and (b) phosphate by PVA/SA-CFZ. Experimental conditions: initially, 100 mg/L ammonium and 100 mg/L phosphate in water; the dosage of PVA/SA-CFZ was 6 g/L; the reaction time was 0 ~ 360 min. Error bars represent min/max values observed for duplicate experiments (too small if not shown).

Table 2 Kinetic parameters for nitrogen and phosphorus removal on PVA/SA-CFZ. Reaction conditions: initially, 100 mg/L ammonium and 100 mg/L phosphate in water; the dosage of PVA/SA-CFZ was 6 g/L; the reaction time was 0 ~ 360 min.

	Pseudo-first-order model			Pseudo-second-order model		
	q_e (mg/g)	k_1 (mg/(g■min)	R^2	q_e (mg/g)	k_2 (g/(mg■min)	R^2
Nitrogen	29.99 ± 0.97	0.02094 ± 0.00252	0.9428	34.41 ± 0.07	0.00079 ± 0.00001	0.9809
Phosphorus	32.91 ± 1.21	0.00611 ± 0.00048	0.9920	47.62 ± 2.50	0.00009 ± 0.00001	0.9923

higher than that of the complexation between phosphate and metal hydroxide.

3.3. Mechanism investigation

XPS analysis was used to investigate the mechanism for P adsorption by PVA/SA-CFZ. O1s spectra can be generally deconvoluted into three peaks at 530.90 eV (O^{2-}), 532.32 eV (Hydroxyl group, M−OH) and 533.03 eV (H_2O) (He et al., 2016; Ma et al., 2015). Normalized relative intensities (%) of XPS O1s peaks showed that the fraction of O^{2-} increased from 17.36% to 25.65% after the P adsorption, instead, the relative intensity of M−OH decreased from 59.12% to 53.09% (Fig. 6**a, b**), which indicated that the complexation between surface hydroxyl group with P converted M−O−OH into M−O−P (He et al., 2016; Xiong et al., 2015). The hydroxyl group on the surface of PVA/SA-CFZ should be the coordination site for P adsorption from aqueous phase. In terms of Fe 2p spectra of PVA/SA-CFZ with and without P adsorption, the peaks at 711.5 eV (Fe 2p 2/3) and 724.3 eV (Fe 2p 1/2) jointly confirmed the presence of FeOOH (Tan et al., 1990) (Fig. 6**c**). After the P adsorption, the peaks of Fe 2p 2/3 and
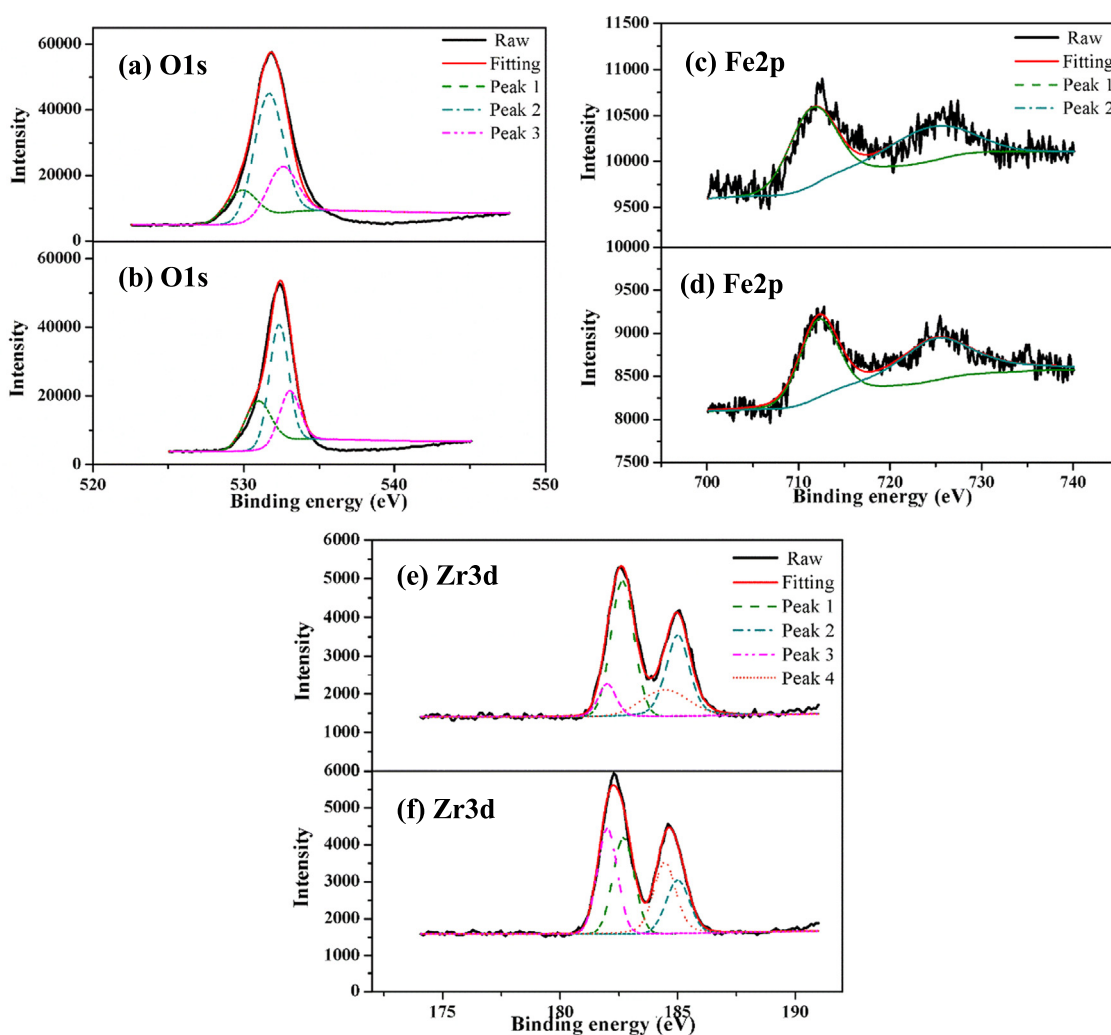
Fig. 6 XPS spectra of PVA/SA-CFZ with (a, c, e) and without (b, d, f) phosphate adsorption. Experimental conditions: initially, 100 mg/L ammonium and 100 mg/L phosphate in water; the dosage of PVA/SA-CFZ was 6 g/L; the reaction time was 360 min.

Fe 2p 1/2 shifted to the 712.2 eV and 724.9 eV, respectively, which corresponded to $FePO_4$ (Bacelo et al., 2020; Li et al., 2020) (Fig. 6d). The chemical shift of Fe 2p peaks to the higher energy binding should be due to the increased formation of Fe–O–P on the surface of PVA/SA-CFZ (Guaya et al., 2016). The four sub-peaks were identified in the spectra of Zr XPS profiles (Fig. 6e, f). The peaks at 182.65 eV and 185.00 eV were attributed to zirconium oxide and zirconium hydroxyl oxide, respectively. After the phosphorus adsorption, these two peaks were found to shift to 182.00 eV and 184.45 eV (Rumble et al., 1992), respectively, since the formation of Zr-O-P would shift the Zr-O peaks to the lower binding energy zone (Fang et al., 2017).

According to the above analysis, the reaction pathways for P fixation by PVA/SA-CFZ are proposed. Primarily, the presence of clinoptilolite in PVA/SA-CFZ provides cation-exchange sites, which should dominate the removal of ammonium from aqueous phase (Du et al., 2005). The hydroxyl groups are introduced on the surface of PVA/SA-CFZ through the formation of FeOOH and ZrOOH. The electrophilicity of metal atom (Fe or Zr) would provide the coordination sites for the lone electron pair of oxygen in phosphate (Wu et al., 2019). As a result, the aqueous phosphate can be captured by the generation of complex unit, M−O−P bonds. This reaction of ligand exchange is the main pathway for phosphate removal. Additionally, the change of pH may lead to the solubilization of Fe/Zr. According to the XPS analysis (Fig. 6d), the formation of $FePO_4$ precipitates also partially contributed to the phosphorus adsorption from aqueous phase (Zhang et al., 2018).

4. Conclusions

In this study, a novel composite absorbent, PVA/SA-CFZ, was successfully synthesized by immobilizing hydrated ferric-zirconium binary oxide precipitate and clinoptilolite powder in the cross-linking of polyvinyl alcohol-alginate covalent. It is confirmed that PVA/SA-CFZ exhibited the excellent performance in both nitrogen and phosphorus removal from aqueous phase over a wide range of pH (4 ~ 11). The adsorption of nitrogen and phosphorus both followed the pseudo-second-order model with the maximum adsorption capacities of 34.41 mg-N/g PVA/SA-CFZ and 47.62 mg-P/g PVA/SA-CFZ, respectively. The mechanism investigation indicated that the removal of ammonium from aqueous phase should be mainly due to the ion-exchange property of clinoptilolite. In contrast, the electrostatic attraction, the inner sphere complexation with M−O−OH groups, and the formation of phosphate precipitation jointly contributed to the fixation of phosphorus by PVA/SA-CFZ. To sum up, PVA/SA-CFZ can serve as a highly effective composite absorbent for the simultaneous removal of aqueous ammonium and phosphate, and would provide a novel option for the enrichment of low-concentration nutrients from wastewater.

Declaration of Competing Interest

The authors declare that they have no known competing financial interests or personal relationships that could have appeared to influence the work reported in this paper.

Appendix A. Supplementary material

Supplementary data to this article can be found online at https://doi.org/10.1016/j.arabjc.2021.103354.

References

Acelas, N.Y., Martin, B.D., López, D., Jefferson, B., 2015. Selective removal of phosphate from wastewater using hydrated metal oxides dispersed within anionic exchange media. Chemosphere 119, 1353–1360.

Bacelo, H., Pintor, A.M.A., Santos, S.C.R., Boaventura, R.A.R., Botelho, C.M.S., 2020. Performance and prospects of different adsorbents for phosphorus uptake and recovery from water. Chem. Eng. J. 381, 122566. https://doi.org/10.1016/j.cej.2019.122566.

Bae, H., Choi, M., Chung, Y.-C., Lee, S., Yoo, Y.J., 2017. Core-shell structured poly(vinyl alcohol)/sodium alginate bead for single-stage autotrophic nitrogen removal. Chem. Eng. J. 322, 408–416.

Barrett, E.P.et al., 1951 The determination of pore volume and area distributions in porous substances. I. Computations from nitrogen isotherms. Journal of the American Chemical Society 73(1), 373-380.

BLANEY, L., CINAR, S., SENGUPTA, A., 2007. Hybrid anion exchanger for trace phosphate removal from water and wastewater. Water Res. 41 (7), 1603–1613.

Bui, T.H., Hong, S.P., Yoon, J., 2018. Development of nanoscale zirconium molybdate embedded anion exchange resin for selective removal of phosphate. Water Res. 134, 22–31.

Chen, T.-H., Wang, J.-Z., Wang, J., Xie, J.-J., Zhu, C.-Z., Zhan, X.-M., 2015. Phosphorus removal from aqueous solutions containing low concentration of phosphate using pyrite calcinate sorbent. Int. J. Environ. Sci. Technol. 12 (3), 885–892.

Chinese Ministry of Environmental Protection (2002) Chinese national standard for the effluent of WWTPs (GB18918).

Cui, H., Li, L.Y., Grace, J.R., 2006. Exploration of remediation of acid rock drainage with clinoptilolite as sorbent in a slurry bubble column for both heavy metal capture and regeneration. Water Res. 40 (18), 3359–3366.

Ding, Shilin, Fang, Dexin, Pang, Zishan, Luo, Bin, Li, Kuang, Wang, Han, Zhang, Qian, Shen, Qiushi, Ji, Fangying, 2018. Immobilization of powdery calcium silicate hydrate via PVA covalent cross-linking process for phosphorus removal. Science of the Total Environment 645, 937–945.

DU, Q., LIU, S., CAO, Z., WANG, Y., 2005. Ammonia removal from aqueous solution using natural Chinese clinoptilolite. Sep. Purif. Technol. 44 (3), 229–234.

Fang, L., Wu, B., Lo, I.M.C., 2017. Fabrication of silica-free superparamagnetic $ZrO_2@Fe_3O_4$ with enhanced phosphate recovery from sewage: performance and adsorption mechanism. Chem. Eng. J. 319, 258–267.

G. Hill, Charles and W. Root, T. 2014 Basic and Applied Aspects of Biochemical Transformations and Bioreactors, John Wiley & Sons, Inc.

Gong, Guozhuo, Ye, Shufeng, Tian, Yajun, Wang, Qi, Ni, Jiandi, Chen, Yunfa, 2009. Preparation of a new sorbent with hydrated lime and blast furnace slag for phosphorus removal from aqueous solution. J. Hazard. Mater. 166 (2-3), 714–719.

Guaya, Diana, Valderrama, César, Farran, Adriana, Cortina, José Luis, 2016. Modification of a natural zeolite with Fe (III) for simultaneous phosphate and ammonium removal from aqueous solutions. J. Chem. Technol. Biotechnol. 91 (6), 1737–1746.

Hach, C., 2002. Water analysis handbook. Loveland, Colorado, USA.

He, Yinhai, Lin, Hai, Dong, Yingbo, Liu, Quanli, Wang, Liang, 2016. Simultaneous removal of ammonium and phosphate by alkaline-activated and lanthanum-impregnated zeolite. Chemosphere 164, 387–395.

Hu, Haifeng, Yang, Liu, Lin, Zhen, Xiang, Xiaotong, Jiang, Xiancai, Hou, Linxi, 2018. Preparation and characterization of novel magnetic Fe_3O_4/chitosan/$Al(OH)_3$ beads and its adsorption for fluoride. Int. J. Biol. Macromol. 114, 256–262.

Ko, Young Gun, Do, Taegu, Chun, Youngsang, Kim, Choong Hyun, Choi, Ung Su, Kim, Jae-Yong, 2016. CeO_2-covered nanofiber for highly efficient removal of phosphorus from aqueous solution. J. Hazard. Mater. 307, 91–98.

Lai, Li, Xie, Qiang, Chi, Lina, Gu, Wei, Wu, Deyi, 2016. Adsorption of phosphate from water by easily separable Fe_3O_4@SiO_2 core/shell magnetic nanoparticles functionalized with hydrous lanthanum oxide. J Colloid Interface Sci 465, 76–82.

Li, Yaorui, Bai, Pu, Yan, Yan, Yan, Wenfu, Shi, Wei, Xu, Ruren, 2019. Removal of Zn^{2+}, Pb^{2+}, Cd^{2+}, and Cu^{2+} from aqueous solution by synthetic clinoptilolite. Microporous and Mesoporous Materials 273, 203–211.

Li, Rui, Li, Qiao, Sun, Xiuyun, Li, Jiansheng, Shen, Jinyou, Han, Weiqing, Wang, Lianjun, 2020. Removal of lead complexes by ferrous phosphate and iron phosphate: Unexpected favorable role of ferrous ions. J. Hazard. Mater. 392, 122509. https://doi.org/10.1016/j.jhazmat.2020.122509.

Liu, Hongbo, Chen, Zihua, Guan, Yongnian, Xu, Suyun, 2018. Role and application of iron in water treatment for nitrogen removal: A review. Chemosphere 204, 51–62.

Liu, Qiu, Zheng, Ping, Zhang, Meng, Yu, Xiaoqing, Abbas, Ghulam, 2015. Phosphorus removal using ferric–calcium complex as precipitant: Parameters optimization and phosphorus-recycling potential. Chemical Engineering Journal 268, 230–235.

Loos, R. et al, 2012. EU wide monitoring survey on waste water treatment plant effluents. JRC Publications Repository, Ispra, Italy.

Ma, L. et al, 2015. Simultaneous adsorption of Cd(II) and phosphate on Al_{13} pillared montmorillonite. RSC Adv. 5 (94), 77227–77234.

Naushad, M., 2014. Surfactant assisted nano-composite cation exchanger: development, characterization and applications for the removal of toxic Pb^{2+} from aqueous medium. Chem. Eng. J. 235, 100–108.

Oguz, E., 2004. Removal of phosphate from aqueous solution with blast furnace slag. J. Hazard. Mater. 114 (1), 131–137.

Prabhu, Subbaiah Muthu, Koilraj, Paulmanickam, Sasaki, Keiko, 2017. Synthesis of sucrose-derived porous carbon-doped $Zr_xLa_{1-x}OOH$ materials and their superior performance for the simultaneous immobilization of arsenite and fluoride from binary systems. Chem. Eng. J. 325, 1–13.

Zhou, Qi, Wang, Xinze, Liu, Jianyong, Zhang, Ling, 2012. Phosphorus removal from wastewater using nano-particulates of hydrated ferric oxide doped activated carbon fiber prepared by Sol-Gel method. Chem. Eng. J. 200–202, 619–626.

Rashidi Nodeh, Hamid, Sereshti, Hassan, Zamiri Afsharian, Elham, Nouri, Nina, 2017. Enhanced removal of phosphate and nitrate ions from aqueous media using nanosized lanthanum hydrous doped on magnetic graphene nanocomposite. J. Environ. Manage. 197, 265–274.

Rumble, J.R., Bickham, D.M., Powell, C.J., 1992. The NIST X-ray photoelectron spectroscopy database. Surf. Interface Anal. 19 (1-12), 241–246.

Tan, B.J. et al., 1990 X-ray photoelectron spectroscopy studies of solvated metal atom dispersed catalysts. Monometallic iron and bimetallic iron-cobalt particles on alumina. Chemistry of Materials 2(2), 186-191.

Tu, Y. et al., 2019 Adsorption of ammonia nitrogen on lignite and its influence on coal water slurry preparation. Fuel, 34-43.

USEPA, 2008. Clean Water Act. United States Environment Protection Agency, Washington DC.

Vassileva, P., Voikova, D., 2009. Investigation on natural and pretreated Bulgarian clinoptilolite for ammonium ions removal from aqueous solutions. J. Hazard. Mater. 170 (2), 948–953.

Wan, Chunli, Ding, Shuai, Zhang, Chen, Tan, Xuejun, Zou, Weiguo, Liu, Xiang, Yang, Xue, 2017. Simultaneous recovery of nitrogen and phosphorus from sludge fermentation liquid by zeolite adsorption: Mechanism and application. Sep. Purif. Technol. 180, 1–12.

Wang, J., Guo, X., 2020. Adsorption isotherm models: Classification, physical meaning, application and solving method. Chemosphere 258, 127279.

Wang, Ya-nan, Tsang, Yiu Fai, Wang, Huawei, Sun, Yingjie, Song, Yi, Pan, Xiangliang, Luo, Siyi, 2020. Effective stabilization of arsenic in contaminated soils with biogenic manganese oxide (BMO) materials. Environ. Pollut. 258, 113481. https://doi.org/10.1016/j.envpol.2019.113481.

Weirich, Scott R., Silverstein, JoAnn, Rajagopalan, Balaji, 2011. Effect of average flow and capacity utilization on effluent water quality from US municipal wastewater treatment facilities. Water Res. 45 (14), 4279–4286.

Wu, B. et al., 2019 Selective phosphate removal from water and wastewater using sorption: process fundamentals and removal mechanisms. Environmental Science & Technology 54(1), 50-66.

Xi, H. et al., 2021 Highly selective adsorption of phosphate from high-salinity water environment using MgO-loaded and sodium alginate-immobilized bentonite beads. Journal of Cleaner Production, 127773.

Xiong, C. et al., 2015 Investigation on the efficiency and mechanism of Cd(II) and Pb(II) removal from aqueous solutions using MgO nanoparticles. Journal of Hazardous Materials 299, 664-674.

Zhang, Gaosheng, Qu, Jiuhui, Liu, Huijuan, Liu, Ruiping, Wu, Rongcheng, 2007. Preparation and evaluation of a novel Fe-Mn binary oxide adsorbent for effective arsenite removal. Water Res. 41 (9), 1921–1928.

Zhang, Xiaolin, Huang, Ping, Zhu, Siyao, Hua, Ming, Pan, Bingcai, 2019a. Nanoconfined hydrated zirconium oxide for selective removal of Cu(II)-carboxyl complexes from high-salinity water via ternary complex formation. Environ. Sci. Technol. 53 (9), 5319–5327.

Zhang, Yanyang, She, Xinwei, Gao, Xiang, Shan, Chao, Pan, Bingcai, 2018. Unexpected favorable role of Ca^{2+} in phosphate removal by using nanosized ferric oxides confined in porous polystyrene beads. Environmental Science & Technology 53 (1), 365–372.

Zhang, Yanyang, She, Xinwei, Gao, Xiang, Shan, Chao, Pan, Bingcai, 2019b. Unexpected favorable role of Ca^{2+} in phosphate removal by using nanosized ferric oxides confined in porous polystyrene beads. Environ. Sci. Technol. 53 (1), 365–372.

Zhou, Kun, Wu, Boran, Dai, Xiaohu, Chai, Xiaoli, 2018. Development of polymeric iron/zirconium-pillared clinoptilolite for simultaneous removal of multiple inorganic contaminants from wastewater. Chem. Eng. J. 347, 819–827.

Zong, Enmin, Liu, Xiaohuan, Wang, Jifu, Yang, Shenxiang, Jiang, Jinhua, Fu, Shenyuan, 2017. Facile preparation and characterization of lanthanum-loaded carboxylated multi-walled carbon nanotubes and their application for the adsorption of phosphate ions. J. Mater. Sci. 52 (12), 7294–7310.